

ON THE SIZE AND MASS OF PHOTO-IONIZED CLOUDS IN EXTENDED SPIRAL GALAXY HALOS

JULIE D. DAVIS, BRIAN A. KEENEY, CHARLES W. DANFORTH, AND JOHN T. STOCKE

Center for Astrophysics and Space Astronomy, Department of Astrophysical and Planetary Sciences, University of Colorado
389 UCB, Boulder, CO 80309; julie.davis@colorado.edu

Draft version June 28, 2021

ABSTRACT

The size and mass of two circum-galactic medium (CGM) clouds in the halo (impact parameter = 65 kpc) of a nearby late-type galaxy, MGC -01-04-005 ($cz = 1865 \text{ km s}^{-1}$), are investigated using a close triplet of QSO sight lines (the “LBQS Triplet”; Crighton et al. 2010). Far ultraviolet spectra obtained with the Cosmic Origins Spectrograph (COS) aboard the *Hubble Space Telescope* (*HST*) find two velocity components in Ly α at ~ 1830 and 1900 km s^{-1} in two of these sight lines, requiring minimum transverse cloud sizes of ≥ 10 kpc. A plausible, but not conclusive, detection of C IV 1548 Å absorption at the higher velocity in the third sight line suggests an even larger lower limit of ≥ 23 kpc for that cloud. Using various combinations of constraints, including photo-ionization modeling for one absorber, lower limits on masses of these two clouds of $\gtrsim 10^6 M_{\odot}$ are obtained. Ground-based imaging and long-slit spectroscopy of MGC -01-04-005 obtained at the Apache Point Observatory (APO) 3.5m telescope find it to be a relatively normal late-type galaxy with a current star formation rate (SFR) of $\sim 0.01 M_{\odot} \text{ yr}^{-1}$. *Galaxy Evolution Explorer* (*GALEX*) photometry finds a SFR only a few times higher over the last 10^8 yrs. We conclude that the CGM clouds probed by these spectra are typical in being at impact parameters of $0.4\text{--}0.5 R_{\text{vir}}$ from a rather typical, non-starbursting late-type galaxy so that these size and mass results should be generic for this class. Therefore, at least some CGM clouds are exceptionally large and massive.

Subject headings: galaxies: halos — galaxies: spiral — intergalactic medium — quasars: absorption lines

1. INTRODUCTION

In the last few years the advent of the high throughput far-UV (FUV) Cosmic Origins Spectrograph (COS; Green et al. 2012) on the *Hubble Space Telescope* (*HST*) has allowed the discovery of a massive and extensive circum-galactic medium (CGM; a.k.a. gaseous halo) around late-type galaxies (Prochaska et al. 2011; Tumlinson et al. 2011, 2013; Stocke et al. 2013; Werk et al. 2013; Borthakur et al. 2013; Stocke et al. 2014; Werk et al. 2014; Bordoloi et al. 2014; Lehner et al. 2015). COS FUV spectroscopy of background, bright QSO targets finds H I often accompanied by low- (e.g., C II, Si II, Si III) and/or high-ion (e.g., C IV, Si IV, and O VI) metal absorption lines at the redshifts of foreground, typically late-type galaxies. The absorptions occur ubiquitously within approximately one projected virial radius (R_{vir} ; see Shull 2014, for a detailed discussion) implying high covering factor (Prochaska et al. 2011; Tumlinson et al. 2011; Stocke et al. 2013) for the CGM around late-type galaxies in the current epoch.

Studies of low- z galaxy halos have been made by targeting QSO/galaxy pairs using *HST*/COS (Tumlinson et al. 2013; Stocke et al. 2013; Bordoloi et al. 2014). Using COS science team Guaranteed Time Observations (GTO), Stocke et al. (2013) studied late-type galaxy halos from extreme dwarfs and low surface brightness galaxies to $\sim L^*$ spirals at impact parameters $\leq 1.5 R_{\text{vir}}$ finding associated H I Ly α absorption in all cases. The COS-Halos research team (Tumlinson et al. 2011, 2013; Werk et al. 2013; Bordoloi et al. 2014) studied both late-type, star forming galaxies and early type galaxies with very low amounts of current star formation. The first COS-

Halos studies were of $L > L^*$ galaxies. The later work of Bordoloi et al. (2014) concentrated on $L = 0.1\text{--}1 L^*$ late-type galaxies along with a few lower luminosity dwarfs. The COS-Halos program targeted sight lines whose impact parameters are $\leq 0.5 R_{\text{vir}}$.

These new *HST*/COS observations were supplemented by the use of archival Space Telescope Imaging Spectrograph (STIS) FUV spectroscopy for a large number of very bright, low- z QSOs in conjunction with ground-based spectroscopic surveys of galaxies near these sight lines (Morris et al. 1993; Bowen et al. 1997; Tripp, Lu, & Savage 1998; Penton, Stocke, & Shull 2002, 2004; Stocke et al. 2006; Prochaska et al. 2011; Stocke et al. 2013). Differing from the targeted surveys mentioned in the previous paragraph, these “serendipitous” studies found absorption systems first, then identified associated galaxies in some cases using the ground-based galaxy redshift surveys. In these “serendipitous” surveys approximately 50% of absorbers with $\log N_{\text{HI}} (\text{cm}^{-2}) \geq 14.0$ are found within the virial radius of an associated galaxy. This percentage decreases with decreasing column density.

These two types of studies (summarized in Stocke et al. 2013) show H I Ly α absorption at comparable redshifts to foreground $L \geq 0.1 L^*$ late-type galaxies at near unity covering factor out to $1\text{--}2 R_{\text{vir}}$. Dwarfs also have significant associated absorption but at lesser ($\sim 50\%$) covering factors within $1\text{--}2 R_{\text{vir}}$. At all luminosities, these covering factors decline quite slowly out to several virial radii making it unclear where the CGM ends and the IGM begins if only Ly α is considered. However, it has been known for some time (e.g., Chen et al. 2001; Stocke et al. 2006) that metal absorption (C IV and O VI in particu-

lar) truncates rather dramatically at ~ 0.3 – 1 Mpc from the nearest bright galaxy. It is plausible but not proven that metal-enriched gas at $Z \gtrsim 0.1 Z_{\odot}$ metallicity occurs only within the confines of spiral-rich galaxy groups (Stocke et al. 2014), which have similar physical extents to this enriched gaseous reservoir. The detection of extensive CGMs around early-type galaxies remains controversial (Thom et al. 2012).

From the initial COS-Halos program results (Tumlinson et al. 2011) it was already clear that these gaseous halos are very massive. However, determining a more accurate mass in photo-ionized halo clouds requires some simple modeling to determine the ionization state, density, and extent of these clouds. This standard photo-ionization modeling has been accomplished by two independent groups who find quite similar but not identical results. Both analyses assume single phase clouds in photo-ionization equilibrium with the extragalactic ionizing radiation, whose amount is fixed assuming the value from Haardt & Madau (2012). If a UV background intensity somewhat stronger than that of Haardt & Madau (2012) is used (see Shull et al. 2015, for a justification for this adjustment), the cloud densities and total masses determined would also increase by a similar factor. By determining the ionization parameter using the line ratios of metal ions in different ionization states, total cloud densities and indicative sizes can be calculated. Cloud masses follow by assuming quasi-spheroidal clouds. Stocke et al. (2013) analyzed 25 systems with at least two adjacent ion states, finding cloud densities and line-of-sight sizes of $n_H = 10^{-3}$ to 10^{-4} cm^{-3} and 0.1–20 kpc, respectively. Werk et al. (2014) analyzed the metal absorption systems in 44 clouds finding somewhat lower densities ($\langle n_H \rangle = 10^{-4.2}$ cm^{-3}) and larger cloud sizes. However, based on the limited number of input spectral line strengths (and their substantial uncertainties) as well as the unlikely assumption that the clouds are homogenous, single-phase gas, the results of these photo-ionization models are quite uncertain. Even in ideal circumstances these models provide only a substantial range for values of cloud density and size (and thus mass). Therefore, other cloud size constraints are required to be able to conclude more definitively that photoionized CGM clouds are large and massive.

From these basic results the inferences derived for the mass of the CGM around a typical $L \geq 0.1 L^*$ late-type galaxy diverge somewhat between these two studies. Werk et al. (2014) advocate for a single-phase CGM with density decreasing only very slowly away from the associated galaxy and $M_{\text{CGM}} = 6.5 \times 10^{10} M_{\odot}$. Stocke et al. (2013) use their 25 observed clouds to construct an ensemble mass ($\sim 10^{10} M_{\odot}$) and a volume filling factor of 3–10%. The latter results yield a significantly lower total CGM mass, leaving a large volume in the CGM unfilled by photo-ionized gas clouds.

Whether the CGM is completely filled with photo-ionized gas or not makes a difference for the interpretation of the detected O VI absorption. In the Werk et al. (2014) analysis the O VI must arise in gas co-mingled with the gas giving rise to the photo-ionized absorption regardless of whether the O VI itself is photo-ionized or collisionally ionized. In the Stocke et al. (2013) picture the photo-ionized clouds are surrounded by a hotter

medium which fills 90–97% of the CGM volume; the interface between the clouds and a hot substrate create the collisionally ionized O VI through shocks. Stocke et al. (2014) claim that broad, shallow O VI absorption discovered in high-S/N COS spectra obtained by the GTO team (Savage et al. 2014) is evidence for this hotter substrate. Unlike the stronger, narrower O VI detected and studied by the COS-Halos Team, this shallower absorption suggests temperatures in the $T = 10^5$ to $10^{6.5}$ K range. An intra-group gas at these temperatures was predicted to be present in spiral-rich groups by Mulchaey et al. (1996), analogous to the hot gas seen in rich clusters and elliptical-dominated rich groups of galaxies (Mulchaey 2000).

New constraints on cloud sizes can distinguish between these two pictures of the CGM, indirectly arguing for or against a very massive, hot, diffuse group gas surrounding these late-type systems. More generally, since the mass of a quasi-spherical cloud scales as cloud size r^3 while the total area of the cloud goes as r^2 , the larger the individual halos clouds, the greater their mass, scaling as r^3/r^2 in the limit of unity covering factor.

In this paper we place constraints on the size of two halo clouds found around a rather normal $\sim 0.1 L^*$ galaxy using a triplet of sight lines closely spaced on the sky (10–23 kpc separation at the galaxy’s Hubble distance of 27 Mpc; see Figure 1). These three closely-spaced QSOs were found in the Large Bright QSO Survey (LBQS; Foltz et al. 1987), designated LBQS 0107–025A,B and LBQS 0107–0232 (referred to collectively as the “LBQS triplet” hereafter) and described in detail in Crighton et al. (2010). In Section 2 we describe the *HST*/COS spectra, concentrating on absorptions found in the three sight lines at $z = 0.00622$. In Section 3 we describe our new observations of galaxy MCG -01-04-005 which bear on its recent star formation history. The discussion in Section 4 focuses on the constraints on cloud size obtained using these observations. In Section 5 we summarize our conclusions.

2. *HST*/COS FUV SPECTROSCOPY OF THE LBQS TRIPLET

Crighton et al. (2010) use the absorption line data from the *HST*/COS FUV spectra of the LBQS triplet to constrain the relationship between galaxies and absorbers at $z < 1$, finding an excess of groups of galaxies compared to expectations. A high column density Lyman limit system (LLS) is present in LBQS 0107–0232 (J0107C hereafter) at $z = 0.557$ and a metal-enriched absorber is found in LBQS 0107–025A,B (J0107A and J0107B hereafter, respectively) at $z = 0.227$, located 200 kpc from a bright galaxy at the same redshift (see Figure 1). Muzahid (2014) used the common O VI absorptions in this system to infer that the O VI-absorbing gas is very large on the sky (600–800 kpc) and must therefore contain a substantial amount of mass ($\geq 10^{11} M_{\odot}$). This inferred mass is similar to the amount inferred by Stocke et al. (2013) to be in the hot CGM phase found by Savage et al. (2014) and Stocke et al. (2014). Muzahid (2014) also analyzed the photo-ionized phase in the $z = 0.227$ absorber, finding evidence that this cooler cloud is quite small (< 1 kpc) suggesting that it is a high velocity cloud imbedded in the hot O VI-absorbing substrate.

The same COS spectra used by Crighton et al. (2010)

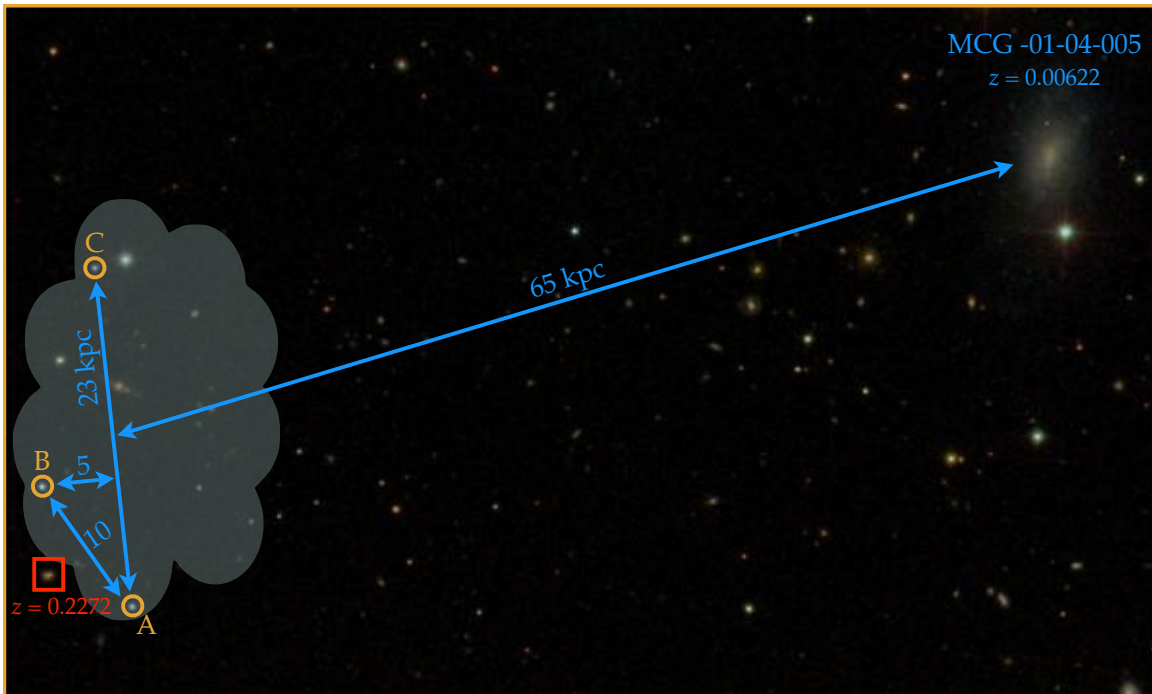


Figure 1. An SDSS finder chart of the region surrounding the three QSO sight lines studied here (see Section 2) on which we have overlaid an illustrative cartoon of the CGM cloud’s extent if detected in all three sight lines. The QSO positions are indicated by the labels A–C, corresponding to the sight line labeling in the text. An indicative physical impact parameter for the QSO sight lines from MCG -01-04-005 (Section 3) is also shown, as well as the distance between the QSO sight lines evaluated at $z = 0.00622$. Finally, the position of the $z = 0.2272$ galaxy identified by Crighton et al. (2010, ; see Section 2) is indicated by a red square. The image field of view is $10' \times 6'$ and its orientation is north up, east left. All unlabeled distances are kiloparsecs.

and Muzahid (2014) were used by this project. All targets were observed with the Cosmic Origins Spectrograph (COS) as part of HST program 11585 (PI: Crighton) in late 2010 and early 2011. J0107A and J0107B were observed with both far-UV, medium resolution gratings COS/G130M ($1135 < \lambda < 1450 \text{ \AA}$) and COS/G160M ($1400 < \lambda < 1795 \text{ \AA}$). J0107C was observed in the COS/G160M grating only due to the LLS discussed above. Observations made at several different grating positions give continuous spectral coverage over the range $1135 < \lambda < 1795 \text{ \AA}$ ($1400 < \lambda < 1795 \text{ \AA}$ for J0107C) at an approximate resolution of $\mathcal{R} = \lambda/\Delta\lambda \approx 18,000$ ($\Delta v \approx 17 \text{ km s}^{-1}$).

The calibrated, one-dimensional spectra for each exposure were obtained from the Mikulski Archive for Space Telescopes (MAST). The individual exposures were then coadded using standard IDL procedures described in detail by Danforth et al. (2010). Briefly, the individual exposures were binned by three pixels, cross-correlated around strong Galactic absorption features, interpolated onto a common wavelength scale, and combined using an exposure-weighted coaddition scheme. The combined spectra shows the expected smooth continuum and narrow absorption features. The data quality varies over the spectral range due to the different sensitivities and exposure times in the two detectors. Total exposures times, median S/N per resolution element, and median flux levels for each grating are given in Table 1.

2.1. Absorption Line Analysis

To establish the extent of the circumgalactic halo clouds around MCG -01-04-005 (systemic radial velocity = $1864 \pm 5 \text{ km s}^{-1}$; Koribalski et al. 2004) we utilize the

Table 1
Summary of HST/COS Observations

Target	z_{em}	Grating	t_{exp}	S/N	Flux
J0107A	0.9570	G130M	28202	14	7×10^{-16}
		G160M	44430	12	7×10^{-16}
J0107B	0.9560	G130M	21239	16	1.0×10^{-15}
		G160M	21149	11	1.3×10^{-15}
J0107C	0.7280	G160M	83433	10	3×10^{-16}

presence or absence of H I Ly α and C IV 1548, 1550 \AA absorption at the host galaxy redshift in the LBQS triplet (see Figure 2 for all detected absorbers at the redshift of MCG -01-04-005).

The H I Ly α absorptions in J0107A and J0107B are best-fit using two components (see Table 2). In velocity space, both sight lines include a component at $\sim 1830 \text{ km s}^{-1}$ and one at $\sim 1900 \text{ km s}^{-1}$. The specific values for these fits can be seen in Table 2. All of the line fits have physically reasonable b -values except the 1836 km s^{-1} component in J0107B, which is weak enough that a broader, physically-plausible, profile is possible within the statistical errors (see Figure 2). Full line profiles based on the Voigt fit parameters in Table 2 are over-plotted as thick solid lines for all absorption features. For the Ly α profiles, the dotted lines indicate the Voigt fits for each component; for the C IV profiles, the thin lines indicate the 1σ uncertainty on these fits. Special care is required when inferring H I column densities from Voigt profile fits to Ly α profiles; we address these concerns in Section 4.1.

The wavelengths of Ly α and C II in J0107C are obscured by a strong, higher redshift LLS. However, in

this case a reasonably strong C IV absorption is visible at $\sim 6\sigma$ in the stronger of the two doublet lines (see Figure 2 third column and Table 2. The velocity of the C IV in J0107C corresponds to within the errors with a comparably strong C IV in J0107B consistent with the $\sim 1900 \text{ km s}^{-1}$ Ly α component. While no C IV is detected in J0107B, the much stronger Ly α absorber in J0107A compared to J0107B means that the $\sim 1900 \text{ km s}^{-1}$ Ly α component can be at a similar metallicity in all three sight lines. The strength of the C IV in J0107C compared with J0107B suggests that a comparably strong Ly α is present at that location, although undetectable due to the higher redshift LLS. Likewise, C II 1335 Å is weakly detected in J0107A & B, consistent with belonging to the higher velocity absorber (see Figure 2).

Due to intervening ISM and Ly α forest lines, several of the C IV candidate lines require de-blending to confirm their presence. At the galaxy’s redshift, and thus in all three spectra, the weaker line of the C IV doublet is blended with Galactic neutral carbon (C I 1560 Å) ISM absorption shown at a velocity of -72 km s^{-1} in Figure 2. We modeled out the neutral Galactic carbon by simultaneously Voigt-fitting other C I transitions in the same spectrum to obtain a C I column density. A model C I profile using the parameters obtained was then subtracted from the blended region of interest. This model has already been removed from the spectra presented in Figure 2. The location of the C I wavelength is noted in the third row of Figure 2.

In J0107B, only a 3σ upper limit on C IV is reported after the C I model was removed. For J0107A & J0107C, we were able to model cleanly the C IV 1548 Å line (a 6σ detection). Particularly for J0107A (see Figure 2) the 1548 Å-derived model seems to fit the de-blended 1550 Å feature, implying that the de-blending process was reasonably successful with only small C I residuals. However, this line more than likely contains additional contaminants besides C I making its parameters less well-determined; i.e., the 1550 Å detection appears too strong for the observed 1548 Å line strength. Table 2 thus lists proxy values for the C IV 1550 Å feature in J0107A based on the values obtained from the 1548 Å measurement.

In J0107C only the stronger C IV line is well-measured at 1560.9 Å due to the presence of Ly α forest lines at other redshifts in the region of the weaker doublet line. Nevertheless, after the C I de-blending, a weak C IV 1550 Å feature does seem to be present between two strong Ly α absorbers. This tentative detection of the weaker C IV doublet line in J0107C is suggestive but not conclusive due to the higher redshift Ly α lines in its vicinity.

With no other definite lines than the C IV 1548 Å identification at the same redshift in J0107C, we must entertain the possibility that this line is actually a spurious, weak feature at a different redshift. Ly α absorbers are by far the most common in the IGM so the alternative interpretation of the 1560.9 Å feature as Ly α at $z = 0.284$ is suggested. The line has an observed equivalent width of $W_\lambda = 96 \pm 44 \text{ mÅ}$ with a fitted $b = 34 \pm 11 \text{ km s}^{-1}$. Interpreted as a weak Ly α absorber on the linear part

of the curve of growth, this corresponds to a rest equivalent width of $74 \pm 34 \text{ mÅ}$, or $\log N_{\text{HI}} = 13.2 \pm 0.2 \text{ cm}^{-2}$. Danforth et al. (2015) find a bivariate distribution of H I absorbers with $d^2\mathcal{N}(\log N)/dz d\log N = 110 \pm 6$ at this column density. Multiplying by a column density bin width equal to the full range of the measurement uncertainty (0.4 dex), gives $dN/dz = 44 \pm 2$, the frequency of H I absorbers per unit redshift with a column density $\log N = 13.2 \pm 0.2$. The 1560.9 Å line is at the right wavelength to be C IV associated with MGG -01-04-005, but we don’t know the precise velocity of the H I absorption in this particular sight line (see Figure 2). Instead, we estimate the velocity range over which it might be expected using the Ly α and C IV absorption from the other two sight lines: $cz = 1860 \pm 50 \text{ km s}^{-1}$. A full-width of 100 km s^{-1} corresponds to $\Delta z = 3.3 \times 10^{-4}$. Multiplying this Δz by the Ly α absorber frequency at that column density and redshift, the probability for finding an unrelated Ly α line by chance at the location of the expected C IV line is $\sim 1.5\%$. This probability scales linearly with the redshift width Δz of the allowed line centroid.

In summary the Ly α and C IV absorption lines in these three sight lines are over-plotted in Figure 3. The Ly α lines in J0107A & J0107B share both velocity components although the lower velocity component is quite weak in J0107B. J0107A & J0107C have C IV absorption which aligns with the higher velocity component and with each other. The velocity and velocity width coincidences between these two features argue in favor of hypothesis that the J0107C feature is also C IV. While the C IV 1548 Å identifications are confirmed by the presence of weak 1550 Å absorption in J0107A & B, the C IV 1548 Å identification in J0107C could instead be an intervening Ly α absorber at a different redshift. Therefore, the higher velocity component is shared by at least two and maybe all three sight lines. The lower velocity component is present in J0107A without doubt and probably present, although weakly, in J0107B. While there is no evidence for the lower redshift component in J0107C, we can not rule out its presence since we have only C IV coverage in that sight line and the lower redshift component appears to be metal-free at the sensitivity level of the COS spectroscopy in-hand.

3. FOREGROUND GALAXY: MCG -01-04-005

The galaxy MCG -01-04-005 lies to the WNW of the LBQS triplet and is projected 8/8 (68 kpc) on the sky from J0107A, 9/1 (71 kpc) from J0107B, and 8/3 (64 kpc) from J0107C (see Figure 1). Its H I 21-cm centroid velocity ($1865 \pm 6 \text{ km s}^{-1}$; Meyer et al. 2004) is in-between the two velocity components detected in FUV absorption (see Section 2.1) and it has a *B*-band luminosity of $\sim 0.07 L^*$ (Doyle et al. 2005).

3.1. Galaxy Imaging and SFR

H α and R-band images of MCG -01-04-005 were obtained in November 2013 using the SPICAM imager on the Apache Point Observatory 3.5m telescope (APO). Six 300 sec exposures in the R-band and six 900 sec exposures in H α (R: 6492 Å, $\Delta\lambda = 1544 \text{ Å}$; H α : 6570 Å, $\Delta\lambda = 75 \text{ Å}$) were acquired under $\sim 1''$ seeing conditions. The narrowband filter covers an area smaller than the detector field-of-view (FOV), yielding an unvignetted FOV

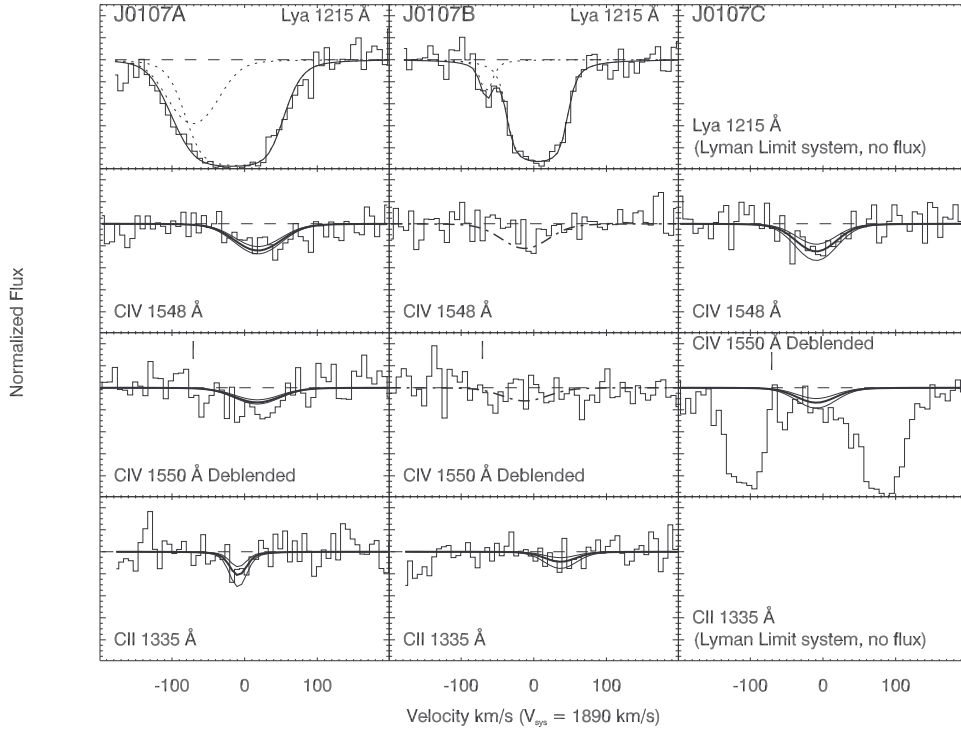


Figure 2. H I Ly α (first row), C IV doublet absorptions (2nd and 3rd rows) and C II (4th row) in all three sight lines, over-plotted with profile fits from Table 2. The components of each Ly α absorption are represented with dotted lines. In J0107A the modeled profile (thick line) with its errors (thin lines) are plotted for the strong C IV doublet line. Direct fits to the weaker doublet line produce column values much too large for the expected doublet ratio, so it is likely that the line is blended with an unknown weak line. Thus a predicted profile based on the measured column density and b-values of the 1548 Å line is plotted instead. The C IV model fits in J0107B (dash-dot lines) represent upper limits centered on the wavelength calculated using J0107A's Ly α redshift. The C IV 1548 Å line in J0107C is also the modeled profile with error bars. The 1550 Å profile in J0107C is a predicted profile like what is displayed for the J0107A weak CIV. In row #3 the Galactic C I line was removed using a profile generated from other Galactic C I lines – the entirety of the region of this subtraction is 1559.6 Å to 1561.7 Å, corresponding to -200 to +200 km s⁻¹. The center of the removed C I profile is noted with a vertical tick mark. Some residuals from the C I deblending may remain in this region. The 4th row displays C II 1335 Å absorption for J0107A and J0107B with modeled profiles overlotted.

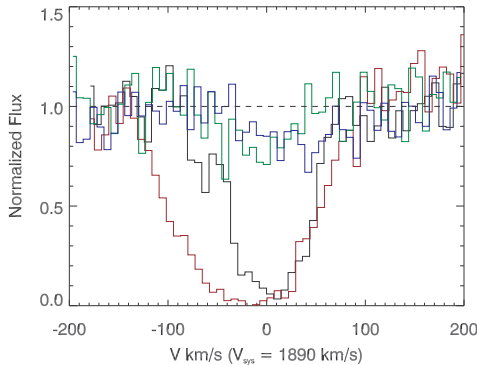


Figure 3. Relative velocities of the absorption systems, using Ly α in J0107A (red) and J0107B (black), and C IV 1548 Å in J0107A (blue) and J0107C (green). The C IV absorptions in J0107A & C have very similar profiles and velocity extents and are associated entirely with the higher velocity Ly α absorption system.

of $\sim 3.5 \times 3.5$, from which the subimage in Figure 4 is extracted. A standard photometric procedure of subtracting a scaled R-band image from the H α image was used to isolate H α emission. In the pure emission-line image, counts from a $42'' \times 62''$ (150×220 pixel; see Figure 4) rectangular area bounding the estimated extent of the galaxy emission were measured. An equal-sized rect-

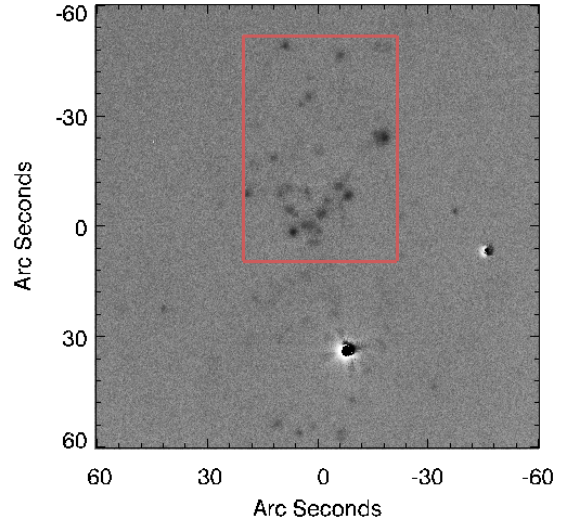


Figure 4. Continuum-subtracted narrowband H α image of MCG -01-04-005. The image has a $2' \times 2'$ field-of-view and is oriented north up, east left. The rectangular region from which the galaxy's H α flux was extracted is indicated. Two bright stars in the field have positive and negative residuals due to changes in the seeing between the exposures.

Table 2
Absorption Table

Target	Species	λ_0 (Å)	λ_{obs} (Å)	cz (km s ⁻¹)	b (km s ⁻¹)	W_λ (mÅ)	$\log N^a$ (cm ⁻²)	σ
J0107A ^b	Ly α	1215.67	1223.09	1830 ± 10	39 ± 9	213 ± 117	13.74 ± 0.09	19.0
...	Ly α	1215.67	1223.33	1888 ± 10	40 ± 5	568 ± 80	14.75 ± 0.20	49.9
...	C IV	1548.20	1558.12	1921 ± 10	50 ± 10	109 ± 18	13.47 ± 0.08	8.2
...	C IV	1550.77	1560.71	1921	40	109	13.47	...
...	C II	1334.53	1342.96	1893 ± 6	12 ± 10	33 ± 21	13.28 ± 0.22	6.6
...	Si II	1260.42	1268.36	...	20	< 25	< 12.2	< 3
...	Si IV	1402.77	1411.61	...	20	< 22	< 12.7	< 3
J0107B ^c	Ly α	1215.67	1223.12	1836 ± 75	4 ± 10	34	13.16	6.2
...	Ly α	1215.67	1223.41	1908 ± 10	17 ± 12	354	15.84	45.0
...	C IV	1548.20	< 57	< 13.43	< 3
...	C IV	1550.77	< 57	< 13.45	< 3
...	C II	1334.53	1343.17	1939 ± 15	27 ± 23	24 ± 22	13.10 ± 0.24	~ 3
...	Si II	1260.42	1268.36	...	20	< 23	< 12.2	< 3
...	Si IV	1402.77	1411.62	1891 ± 10	21 ± 10	36 ± 22	12.95 ± 0.20	3.2
J0107C ^d	C IV	1548.20	1557.97	1893 ± 7	34 ± 11	96 ± 44	13.43 ± 0.15	8.8
...	C IV	1550.77	...	1893	34	96	13.43	...

^a The errors on $\log N$ represent formal fitting errors from χ^2 minimization. We have reason to believe the errors on $\log N_{\text{HI}}$ are actually much larger, as discussed in Section 4.

^b The weak line of the CIV doublet is assumed to be blended with an unknown weak line, as Voigt fitting results in a column density that is too high given known line ratios for CIV. We adopt the strong doublet line values for the 1550 Å line as a reasonable proxy.

^c Since the CIV values for this sight line are upper limits, the observed wavelengths are based on the host galaxy redshift and assumed to be 1558.07 Å and 1560.50 Å. These have been used as the profile centers in Figure 2.

^d The weak line of the CIV doublet is highly blended with unidentified lines and thus no measurement was made, so we follow the same procedure as footnote b.

angular sky region from the same image was subtracted. Assuming appropriate background subtraction and Poissonian error statistics, the resulting galaxy H α count rate was 54 ± 1 cts s⁻¹. However, our H α count rate is contaminated by [N II] emission that closely flanks H α and thus falls within the filter bandpass. To remove this, optical spectra of MCG -01-04-005 were obtained on the same night with the Dual Imaging Spectrograph (DIS) at APO. The two [N II] emission features flanking the H α emission peak were measured and the ratio of emission was found to be $F(\text{NII})/F(\text{H}\alpha) = 0.31$. Therefore our corrected pure H α count rate is 37 ± 1 cts s⁻¹.

Using the standard star BD+28 4211 to flux calibrate, an observed H α flux of $(2.09 \pm 0.06) \times 10^{-14}$ ergs s⁻¹ cm⁻² was measured for the galaxy. Galactic foreground extinction was determined using the extinction law of Fitzpatrick (1999) assuming $R_V = 3.1$ and $E(B - V) = 0.043 \pm 0.006$ mag (Schafly & Finkbeiner 2011), yielding an extinction-corrected H α flux of $(2.29 \pm 0.07) \times 10^{-14}$ ergs s⁻¹ cm⁻²; no extinction intrinsic to MCG -01-04-005 was assumed. We use a luminosity distance of ~ 27 Mpc (Bennet et al. 2013) (also consistent with Tully et al. (2008) distance measurements to an equivalently redshifted galaxy group). This corresponds to a luminosity of $L_{\text{H}\alpha} = (1.99 \pm 0.06) \times 10^{39}$ ergs s⁻¹. Using the calibration of Hunter, Elmegreen, & Ludka (2010) we obtain a current SFR of $\approx 0.01 M_\odot \text{ yr}^{-1}$.

We can also infer a galaxy’s recent SFR from its FUV luminosity. MCG -01-04-005 was observed by the *Galaxy Evolution Explorer* (GALEX) in both the FUV and NUV imaging bands as part of its All Sky Imaging Survey. These shallow (108 sec) exposures found a GALEX FUV magnitude of 17.31 ± 0.08 for MCG -01-04-005 (we have incorporated the absolute photometric uncertainty of GALEX into this magnitude uncertainty; Morrissey et al.

2007), which corresponds to an extinction-corrected luminosity of $L_{\text{FUV}} = (5.1 \pm 0.4) \times 10^{26}$ ergs s⁻¹ Hz⁻¹ using the procedure outlined above. This luminosity implies that the galaxy’s SFR is $\approx 0.06 M_\odot \text{ yr}^{-1}$ (Hunter et al. 2010), ~ 6 times higher than the H α -derived value.

The higher SFR derived from the GALEX FUV luminosity is not surprising since H α measures star formation over the past 10 Myr, whereas FUV luminosity measures star formation in the past 10–100 Myr (Hunter et al. 2010). Nevertheless, as evidenced by its low H α - and FUV-inferred SFRs, MCG -01-04-005 is not currently a starburst galaxy nor has it been one in the recent past. All indications are that it is a rather normal $L \sim 0.1 L^*$ galaxy.

4. SIZE OF A TYPICAL PHOTO-IONIZED HALO CLOUD

These three sight lines present the opportunity to obtain limits on the physical extent of two typical late-type galaxy halo clouds. From the aspect of its SFR, MCG -01-04-005 appears to be entirely normal, certainly not a starburst, over the recent past. The impact parameter for these sight lines is a modest number of disk radii and only 0.4–0.5 R_{vir} (based on a halo-matching formalism; Stocke et al. 2013). This is comparable to or less than the 0.5–1 R_{vir} region for which very high covering factors in Ly α and/or O VI are found around late-type galaxies (Tumlinson et al. 2011; Stocke et al. 2013; Bordoloi et al. 2014). Therefore, this situation appears entirely typical for the study of photo-ionized halo clouds around late-type galaxies.

There are two velocity components to the Ly α absorption, which are present in two sight lines: J0107A and J0107B, separated by 10 kpc at the distance of MCG -01-04-005. This match sets firm lower limits on the transverse sizes on the sky of these two clouds. While Ly α is quite strong in both sight lines for the ~ 1900 km s⁻¹

absorber, the lower velocity ($\sim 1830 \text{ km s}^{-1}$) Ly α absorption in J0107B is so much weaker than in J0107A that the lower velocity cloud may be only slightly $> 10 \text{ kpc}$ in extent on the sky. These firm lower limits are already larger than most of the CGM cloud sizes inferred by Stocke et al. (2013) and near the median value for the sizes inferred by Werk et al. (2014). Assuming a typical CGM cloud total hydrogen density of $n_{\text{H}} = 10^{-3.5} \text{ cm}^{-3}$ for a spherical CGM cloud yields a lower limit on the mass of these two clouds: $\gtrsim 4.5 \times 10^6 M_{\odot}$. However, additional information is available that bears on the sizes and masses of these clouds.

For the J0107C sight line, the absorption due to these clouds is ambiguous due to the presence of a LLS at higher redshift which obscures the portion of the UV spectrum which contains Ly α associated with MCG -01-04-005. However, in this case there is a shallow absorption present at just the right velocity to be C IV 1548 Å in the $\sim 1900 \text{ km s}^{-1}$ absorber. Additionally, this feature has a similar line width to the C IV found in the J0107A sight line (see Figure 3), so that C IV is a very plausible identification for this feature. However, we cannot rule out entirely that this absorption line could be Ly α at a higher redshift, although the probability of such a chance coincidence is small ($< 2\%$). Additionally, there is a marginal detection of C IV 1550 Å in J01017C which falls between two strong, intervening Ly α absorbers. Therefore, only slightly more speculatively, we conclude that the higher velocity ($\sim 1900 \text{ km s}^{-1}$) cloud extends $> 23 \text{ kpc}$ on the sky. While we can use this limit as the minimum cloud extent in one dimension (approximately tangential to the impact parameter vector; see Figure 1), we do not know the other dimensions explicitly. A plausible lower size limit for the other dimension on the plane of the sky can be set at $\geq 5 \text{ kpc}$ using the distance from the J0107B sight line to the cord connecting sight lines A and C (since our observations suggest a continuous absorption between sight lines A & C; see Figure 1). Assuming an ellipsoidal cloud with axes of $5 \text{ kpc} \times 5 \text{ kpc} \times 23 \text{ kpc}$ finds a minimum mass of $\gtrsim 5 \times 10^6 M_{\odot}$. Assuming $> 23 \text{ kpc}$ for all three dimensions of this cloud, results in nearly a $10^8 M_{\odot}$ lower limit.

4.1. Uncertainties in H I Column Density

In Section 4.2 we will use *CLOUDY* (Ferland et al. 1998) photo-ionization models to attempt to constrain the line-of-sight thickness of the $\sim 1900 \text{ km s}^{-1}$ absorber in J0107A. *CLOUDY* outputs rely on accurate absorption-line measurements, but the N_{HI} value from our Voigt profile fits requires re-evaluation as the Ly α profile is slightly saturated in both velocity components and spectroscopy of the higher-order Lyman lines is not available in this case. The values listed in Table 2 for the Ly α line are the values that minimize the χ^2 of the Voigt-profile fit, but since we are on the flat part of the curve of growth there is a very large uncertainty in column density and b -value for a given equivalent width.

Thus, we will treat the H I column density listed in Table 2 for the $\sim 1900 \text{ km s}^{-1}$ absorber as untrustworthy and estimate its value indirectly. This is unfortunate but unavoidable when the only H I line that can be fit is a saturated Ly α profile with no damping wings.

A famous precedent from the literature may help illustrate this point. Weymann et al. (1995) observed 3C 273 with *HST*/GHRS using the G160M grating and found a best-fit Voigt profile with $\log N_{\text{HI}} = 14.22 \pm 0.07$ and $b = 34 \pm 3 \text{ km s}^{-1}$ for the $\sim 1585 \text{ km s}^{-1}$ Ly α absorber associated with the Virgo cluster. We note that the S/N and spectral resolution of this *HST*/GHRS spectrum of 3C 273 are comparable to those of the *HST*/COS spectrum of J0107A and the best-fit parameters from the Ly α fits are comparable as well. Later, *Far-Ultraviolet Spectroscopic Explorer* (*FUSE*) data became available for 3C 273 and absorption from Ly β -Ly θ were found at the same redshift (Sembach et al. 2001). When a curve-of-growth was generated from these higher-order Lyman series lines Sembach et al. (2001) found $\log N_{\text{HI}} = 15.85^{+0.10}_{-0.08}$ and $b = 16 \pm 1 \text{ km s}^{-1}$. The b -value was reduced by a factor of 2 compared to the initial Weymann et al. (1995) value and the column density increased by a factor of more than 40! Sembach et al. (2001) attributed the discrepancy partially to very low column density component structure that affects the Ly α profile but is undetectable in the higher-order Lyman series lines. Therefore, we must treat an N_{HI} value obtained from Ly α profile fitting alone as uncertain, very likely a lower limit, unless other physical constraints can be identified.

Since N_{HI} is underconstrained by the COS data alone, we have imposed the condition that the J0107A absorber metallicity should be consistent with the galaxy metallicity. This is reasonable because there are no other bright galaxies close to MCG -01-04-005; the nearest brighter galaxy is NGC 448, an $0.6 L^*$ S0 galaxy $\sim 750 \text{ kpc}$ away on the sky. This distance on the sky is nearly $5 \times$ the virial radius for NGC 448 and close to the maximum distance that metals have been detected from any bright galaxy in the current epoch (Stocke et al. 2006, 2013). We conclude that any metals present in these absorbers have originated in MCG -04-01-005. If gas expelled by MCG -04-01-005 mixed with IGM gas it could have an even lower metallicity and an even higher N_{HI} . However, such extreme values do not give Ly α profile fits consistent with the COS spectrum of J0107A nor do they satisfy the photo-ionization modeling requirements presented below.

We have measured a metallicity for MCG -01-04-005 of $[\text{O}/\text{H}] = -0.15 \pm 0.19$ (i.e., $Z_{\text{gal}} \sim 0.7 Z_{\odot}$) using our APO/DIS long slit spectrum (see Section 3.1) with the N2 index calibration of Pettini & Pagel (2004) and the solar oxygen abundance of Asplund et al. (2009). For the absorber metallicity to be consistent with the galaxy metallicity, $\log(Z_{\text{abs}}/Z_{\odot}) = -0.53$ to 0.23 (i.e., within 2σ of the galaxy's nominal value of $[\text{O}/\text{H}] = -0.15$, or the 95% confidence band). To satisfy this constraint the H I column density of the $\sim 1900 \text{ km s}^{-1}$ absorber in J0107A must lie in the range $\log N_{\text{HI}} \approx 15.5 \pm 0.5$. In the photo-ionization models that follow, this range of values can reproduce all of the observed metal-line columns and limits; i.e., for lower H I columns the C II detection implies a metallicity that is too high and for higher H I columns the Si II and Si IV upper limits imply a metallicity that is below this range.

4.2. Photo-ionization Modeling

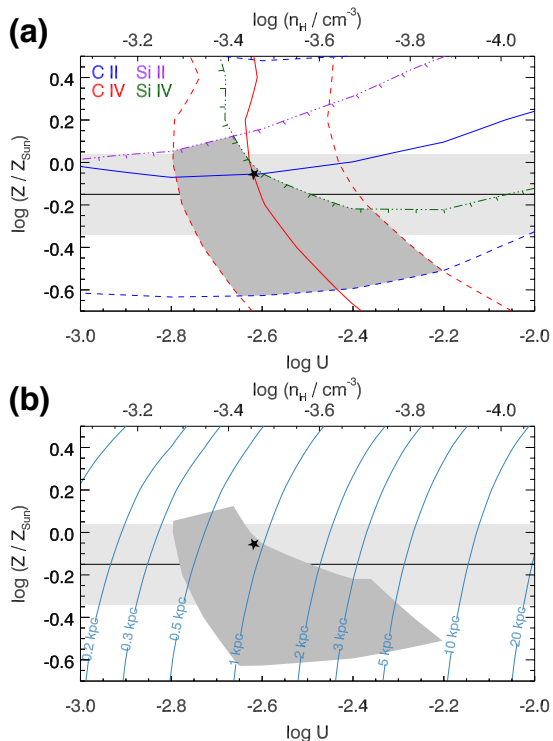


Figure 5. *Top:* The range of *CLOUDY* models that satisfy all of the metal-line constraints for the $\sim 1900 \text{ km s}^{-1}$ absorber toward J0107A with an assumed H I column of $\log N_{\text{HI}} = 15.5 \pm 0.5$ (see text). The allowed model region is shown shaded in gray with the various line constraints color-coded as in the Figure legend. The solid horizontal lines are the plausible metallicity limits set by the galaxy metallicity. *Bottom:* Contours of constant line-of-sight thickness, t , for the *CLOUDY* model in the top panel. The shaded region and metallicity indicators are the same as above.

In this sub-Section we use *CLOUDY* photo-ionization modeling both to obtain additional size constraints for the $\sim 1900 \text{ km s}^{-1}$ absorber in J0107A and also to show that such size constraints are quite uncertain using the minimal data in-hand: N_{HI} , N_{CII} , N_{CIV} , and limits on the column densities of Si II, and Si IV (see Table 2). We use a plane-parallel *CLOUDY* model irradiated by the extragalactic ionizing field as specified by Haardt & Madau (2012) to search for a single-phase solution that self-consistently reproduces the measured column densities and limits. We assume that all species are solely photo-ionized and examine the temperature, T , hydrogen density, n_{H} , neutral fraction, f_{HI} , and line-of-sight thickness, t , of the modeled cloud as a function of ionization parameter, $U = n_{\gamma}/n_{\text{H}}$, and metallicity, Z .

Since the H I column density derived from our Voigt profile fits to Ly α is very uncertain, we use the *CLOUDY* models to constrain N_{HI} using the measured column densities of C II and C IV, and the upper limits on the Si II and Si IV columns as discussed in Section 4.1. Our primary interest is in the range of allowable ionization parameters that these data support, and the line-of-sight thicknesses that can be derived from these values, not the absorber metallicity, which we use only to constrain N_{HI} .

The *CLOUDY* models associated with this revised column density for the $\sim 1900 \text{ km s}^{-1}$ component in J0107A ($\log N_{\text{HI}} = 15.5 \pm 0.5$) are shown in Figure 5a. The metallicity of MCG -01-04-005 is shown as a solid horizontal

line with a light gray band indicating its 2σ uncertainty. The curved solid lines indicate the region of parameter space consistent with the measured C II and C IV column densities, with the flanking dashed lines showing the 1σ uncertainties in the measured columns modulo the very large uncertainty in the H I column. The dot-dashed lines show the upper limits on the Si II and Si IV columns with the tick marks pointing toward the allowable region of parameter space. The filled gray area shows the region of parameter space that is consistent with all of the constraints and the star indicates the fiducial solution where the measured C II and C IV columns agree exactly.

From this model we estimate that $\log U = -2.6^{+0.4}_{-0.2}$ for this absorber; the large uncertainty reflects the large uncertainty in N_{HI} . At the fiducial solution we find $T \sim 11,000 \text{ K}$, $n_{\text{H}} \sim 3 \times 10^{-4} \text{ cm}^{-3}$, $f_{\text{HI}} \sim 0.3\%$, and $t \sim 1 \text{ kpc}$. The range of line-of-sight thicknesses allowed by our *CLOUDY* model is shown in Figure 5b, which displays the same shaded region and metallicity indicators as Figure 5a with contours of constant cloud thickness overlaid. From this plot we conclude that the indicative cloud thickness is $\approx 0.5\text{--}5 \text{ kpc}$.

Guided by the fiducial cloud thickness (1 kpc) and cloud density ($3 \times 10^{-4} \text{ cm}^{-3}$) from the *CLOUDY* models and the cloud size limit ($> 10 \text{ kpc}$) on the sky from the common absorbers, a constant density ellipsoidal cloud with minimum sizes of 1 and 10 kpc in two of the three dimensions is suggested. Assuming 10 kpc for the third cloud dimension (second transverse dimension on the sky) finds a rough cloud mass limit of $\gtrsim 3 \times 10^5 M_{\odot}$. Allowing lower density and larger volume models as in Figure 5 does not change this limit appreciably. However, if our presumed C IV identification for the absorption line detected in Q0107C is correct, the lower mass limit inferred for this spheroidal model is a factor of 4 larger.

In summary, for all cases described in this Section, **most lower limits on cloud mass** are in the range $0.3\text{--}5 \times 10^6 M_{\odot}$. If we had to rely on photo-ionization modeling alone, then the inferred mass would be about $100\times$ less than this lower limit by assuming that each cloud dimension is $\sim 1 \text{ kpc}$. Clearly, the physical limits derived from multiple sight lines are extremely valuable in estimating CGM cloud parameters.

While these values make various assumptions to arrive at a lower mass limit, each of these limiting values for CGM cloud masses are better constrained than those found in either Stocke et al. (2013) or Werk et al. (2014) based solely on simple *CLOUDY* photo-ionization modeling. However, the current result supports the contention made by those authors that at least some CGM clouds have very large sizes and masses. And while we cannot, on the basis of current data, entirely rule out the contention of Werk et al. (2014) that the photo-ionized phase is a monolithic structure around each late-type galaxy, the limited size on the sky of $\sim 10 \text{ kpc}$ for the lower velocity absorber argues weakly against that model.

5. CONCLUSIONS

Using three neighboring QSO sight lines called the LBQS Triplet we have determined that two photo-ionized CGM gas clouds in the halo of the $\sim 0.1 L^*$ late-type galaxy MCG -01-04-005 have physical extents on the sky of $\geq 10 \text{ kpc}$ and total masses $\geq 3 \times 10^5 M_{\odot}$. Most size

constraints available using common absorptions in the COS FUV spectra of the LBQS Triplet require minimum masses of $> 10^6 M_{\odot}$. Given that MCG -01-04-005 is a typical, non-starburst low-luminosity galaxy, and that the impact parameters for these absorbers are typical for CGM absorbers at $0.4\text{--}0.5 R_{\text{vir}}$, we argue that these results also are typical for photo-ionized CGM clouds in general. Therefore, these results support inferences by Tumlinson et al. (2011), Stocke et al. (2013), Werk et al. (2014), and others that individual CGM clouds can be very massive and the ensemble of such clouds contains a significant baryon reservoir, comparable to the mass in a galaxy's stars or larger! The following results led us to these conclusions and represent the main observational findings of this paper.

1. The absorption line data from the *HST*/COS FUV spectra of the LBQS Triplet (J0107A,B,C) finds common absorption at $z = 0.0063$ in two velocity components (~ 1830 and 1900 km s^{-1}) as follows: Ly α in J0107A,B; C IV in J0107A,C; C II in J0107A,B; and upper limits for C IV in J0107B, Si II and Si IV in J0107A,B. The common Ly α and C IV absorptions support minimum cloud sizes for both velocity components of ≥ 10 kpc. A more speculative detection of C IV 1548 Å in J0107C suggests an even larger size limit of ≥ 23 kpc. The measured values for the absorption line detections can be found in Table 2.
2. Using ground-based H α and space-based *GALEX* imaging, we find that the star formation rate in MCG -01-04-005 is small (between $\approx 0.01\text{--}0.06 M_{\odot} \text{ yr}^{-1}$) in the last 100 million years. We conclude that the galaxy is a normal, low luminosity late-type galaxy which has not had a significant starburst in the last 10^8 years at least.
3. Using C II and C IV detections and limits on Si II and Si IV at $\sim 1900 \text{ km s}^{-1}$ in J0107A, single-phase photo-ionization models have been constructed imposing $Z_{\text{abs}} \sim Z_{\text{gal}}$ to limit the range of acceptable H I columns (Section 4). These *CLOUDY* models find $\log U = -2.6^{+0.4}_{-0.2}$ for this absorber and derived physical quantities of $n_{\text{H}} \sim 3 \times 10^{-4} \text{ cm}^{-3}$, $f_{\text{HI}} \sim 0.3\%$, and $t \sim 1$ kpc. While this thickness (t) is smaller than the minimum size on the sky obtained from the common absorptions, the range of cloud thicknesses allowed by the *CLOUDY* models is consistent with an ellipsoidal cloud. However, these models are quite uncertain providing only indicative results on cloud thickness. The common absorptions in the three sight lines provide much better constraints requiring large cloud sizes and masses.
4. Since the common absorptions provide only firm lower limits on transverse clouds size, these observations cannot rule out the presence of a monolithic photoionized phase gas around this galaxy. But the absence of C IV absorption at $\sim 1830 \text{ km s}^{-1}$ in J0107C and the weakness of the Ly α absorption at this velocity in J0107B argue weakly against that model (Werk et al. 2014) by suggesting a cloud size not much larger than 10 kpc for that absorber.

Simon Morris and Neil Creighton are thanked for obtaining the excellent *HST*/COS spectra used for this investigation. We thank the Apache Point Observatory (APO) for making available 3.5m observing time to obtain images and long-slit spectra of MCG -01-04-005. The authors thank the National Science Foundation for support of this research at the University of Colorado through grant AST 1109117.

Facilities: HST (COS), GALEX, APO 3.5m

REFERENCES

- Asplund, M., Grevesse, N., Sauval, A. J., & Scott, P. 2009, *ARA&A*, 47, 481
- Bennet, C. L., Larson, D., Weiland, J. L., et al. 2013, *ApJS*, 208, 20
- Bordoloi, R., Tumlinson, J. T., Werk, J. K., et al. 2014, *ApJ*, 796, 136
- Borthakur, S., Heckman, T., Strickland, D. et al. 2013, *ApJ*, 768, 18
- Bowen, D. V., Tolstoy, E., Ferrara, A., Blades, J. C., & Brinks, E. 1997, *ApJ*, 478, 530
- Chen, H.-W., Lanzetta, K. M., & Webb, J. K. 2001, *ApJ*, 556, 158
- Chen, H.-W. & Mulchaey, J. S. 2009, *ApJ*, 701, 1219
- Crighton, N. H. M., Morris, S. L., Bechtold, J., et al. 2010, *MNRAS*, 402, 1273
- Danforth, C. W. & Shull, J. M. 2008, *ApJ*, 679, 194
- Danforth, C. W., Keeney, B. A., Stocke, J. T., Shull, J. M., & Yao, Y. 2010, *ApJ*, 720, 976
- danforth, C.W., Tilton, E.M., Shull, J.M., et al. 2015, *ApJ* submitted; 2014arXiv1402.2655D
- Doyle, M. T., Drinkwater, M. J., Rohde, D. J., et al. 2005, *MNRAS*, 361, 34
- Ferland, G. J., Korista, K. T., Verner, D. A., et al. 1998, *PASP*, 110, 761
- Fitzpatrick, E. L. 1999, *PASP*, 111, 63
- Foltz, C. B., Chaffee, F. H., Hewett, P. C., et al. 1987, *AJ*, 94, 1423
- Green, J. C., Froning, C. S., Osterman, S., et al. 2012, *ApJ*, 744, 60
- Haardt, F. & Madau, P. 2012, *ApJ*, 746, 125
- Hunter, D. A., Elmegreen, B. G., & Ludka, B. C. 2010, *AJ*, 139, 447
- Keeney, B. A., Stocke, J. T., Rosenberg, J. L., et al. 2013, *ApJ*, 765, 27
- Koribalski, B.S., Staveland-Smith, L., Kilborn, S.D. et al. 2004, *AJ*, 128, 16
- Lehner, N., Howk, J.C., & Wakker, B.P. 2015, *ApJ*, 804, 79
- Meyer, M. J., Zwaan, M. A., Webster, R. L., et al. 2004, *MNRAS*, 350, 1195
- Morris, S. L., Weymann, R. J., Dressler, A., et al. 1993, *ApJ*, 419, 524
- Morrissey, P., Conrow, T., Barlow, T. A., et al. 2007, *ApJS*, 173, 682
- Mulchaey, J. S., Mushotzky, R. F., Burstein, D., & Davis, D. S. 1996, *ApJ*, 456, L5
- Mulchaey, J. S. 2000, *ARA&A*, 38, 289
- Muzahid, S. 2014, *ApJ*, 784, 5
- Penton, S. V., Stocke, J. T., & Shull, J. M. 2002, *ApJ*, 565, 720
- Penton, S. V., Stocke, J. T., & Shull, J. M. 2004, *ApJS*, 152, 29
- Pettini, M. & Pagel, B. E. J. 2004, *MNRAS*, 348, L59
- Prochaska, J. S., Weiner, B., Chan, H.-W., Cooksey, K., & Mulchaey, J. 2011, *ApJS*, 193, 28
- Savage, B. D., Kim, T.-S., Wakker, B. P., et al. 2014, *ApJS*, 212, 8
- Schafly, E. F. & Finkbeiner, D. P. 2011, *ApJ*, 737, 103
- Sembach, K. R., Howk, J. C., Savage, B. D., Shull, J. M., & Oegerle, W. R. 2003, *ApJ*, 561, 573
- Shull, J. M. 2014, *ApJ*, 784, 142
- Shull, J. M., Maloney, J., Danforth, C. D., & Tilton, E. M., 2015, *ApJ*, in press (arXiv:1502.00637)
- Stocke, J. T., Penton, S. V., Danforth, C. W., et al. 2006, *ApJ*, 641, 217
- Stocke, J. T., Keeney, B. A., Danforth, C. W., et al. 2013, *ApJ*, 763, 148

- Stocke, J. T., Keeney, B. A., Danforth, C. W., et al. 2014, ApJ, 791, 128
- Thom, C., Tumlinson, J., Werk, J. K., et al. 2012, ApJ, 758, L41
- Tripp, T. M., Lu, L., & Savage, B. D. 1998, ApJ, 508, 200
- Tully, R. B., Shaya, E. J., Karachentsev, I. D., et al. 2008, ApJ, 676, 184
- Tumlinson, J., Thom, C., Werk, J. K., et al. 2011, Science, 334, 948
- Tumlinson, J., Thom, C., Werk, J. K., et al. 2013, ApJ, 777, 59
- Werk, J., Prochaska, J. X., Thom, C., et al. 2013, ApJS, 204, 17
- Werk, J., Prochaska, J. X., Tumlinson, J. T., et al. 2014, ApJ, 792, 8
- Weymann, R., Rauch, M., Williams, R., Morris, S., & Heap, S. 1995, ApJ, 438, 650